Surface Review and Letters, Vol. 29, No. 4 (2022) 2250043 (8 pages)

DOI: 10.1142/S0218625X22500433

World Scientific
www.worldscientific.com

METALLOGRAPHIC STUDY AND WEAR BEHAVIOR OF Cu-BASED FeTi-REINFORCED COMPOSITES

SERDAR OSMAN YILMAZ*, TANJU TEKER[†,§,] and SENCER SÜREYYA KARABEYOĞLU[‡]

*Department of Mechanical Engineering
Faculty of Engineering, Tekirdağ Namık Kemal University
59160 Çorlu, Tekirdağ, Turkey

[†]Department of Manufacturing Engineering
Faculty of Technology, Sivas Cumhuriyet University
58140 Sivas, Turkey

[‡]Department of Mechanical Engineering
Faculty of Engineering, Kırklareli University
39020 Kırklareli, Turkey
[§]tanjuteker@cumhuriyet.edu.tr

Received 5 September 2021
Revised 21 December 2021
Accepted 23 December 2021
Published 31 January 2022

Cu-based FeTi-reinforced metal matrix composites (MMCs) were produced with FeTi reinforcement additions of 6, 9, 12, 15 and 18 wt.% by powder metallurgy. Microstructural characterization of Cu-based FeTi-reinforced composites was made by using scanning electron microscopy, energy-dispersive spectroscopy, X-ray diffraction and hardness test. The effect of sintering temperatures on the densification of the synthesized powders was investigated. Sliding analyses were conducted to determine the wear behavior. The interface microstructure between FeTi and Cu at 1000°C showed a significant difference. The hardness changed proportionally with the increase in the FeTi particles. The formation of the intermetallic phases CuTi, $CuTi_2$, Cu_4Ti_3 and $TiCu_4$ after sintering caused a higher wear resistance. A 75% reduction in wear rate was achieved by adding 18-wt.% FeTi to pure copper powder.

Keywords: Powder metallurgy; composite; copper; FeTi; hardness; wear.

1. Introduction

Copper (Cu) is preferred due to its high electrical and thermal conductivities, ease of fabrication, high melting point and good corrosion performance.[1,2] Small amounts of ceramic reinforcements dispersed in the copper matrix significantly increased the strength and wear properties. Ceramic particles such as oxides, carbides and borides are used to add more strength to pure copper. Copper alloyed with ceramic particles is largely used in the manufacturing of welding electrodes, engine sets, airframe and electric connections.[3–5] Titanium–copper (Ti–Cu) alloys are preferred over the Cu–Be alloy, which is commonly used in electronic components in the form of connectors

§Corresponding author.

Table 1. The process conditions of the experiment samples.

Sample nos.	S1	S2	S3	S4	S5	S6	S7	S8	S9	S10	S11	S12
Cu (wt.%)	Bal.	Bal.	Bal.	Bal.	Bal.	Bal.	Bal.	Bal.	Bal.	Bal.	Bal.	Bal.
FeTi (wt.%)	12	12	12	12	12	12	12	6	9	12	15	18
Sintering (°C)	600	700	800	850	900	950	1000	900	900	900	900	900

and relay controls.[6,7] High-performance alloys can be manufactured by utilizing the wear resistance of hard phases and the energy absorption properties of soft phase.[8] Hard particles and dispersed carbides transfer the sliding energy to the soft matrix and the energy consumed for wear is decreased. Ti–Cu intermetallic compounds are advanced technological materials with hardness. They improve the properties thus resulting in good sound absorption and high electrical conductivity and biocompatibility. There are studies on the tribological properties of intermetallic compounds as new wear-resistant materials.[9–11] Due to the magnetic shielding performance of Fe, Cu–FeTi (ferro titanium) alloys with more than 20% of Fe content are very popular in the field of marine communications. More than 30% of Fe provides high electromagnetic shielding and corrosion resistance, and it is preferred in the heat sink parts of communication equipment.[10] The Cu–Fe alloy forms two liquid regions rich in Cu and Fe during solidification. This leads to macrosegregation and inhomogeneity of the Cu–Fe alloy after solidification. In the conventional casting, the increase in Fe quantity causes the macroscopic separation of the Fe phase. Therefore, a homogeneous Cu–TiFe alloy can be produced by powder metallurgy.[11] Božić *et al.* reported that the Cu–Ti–TiB_2 composite can be hardened by aging. The metastable Cu_4Ti and TiB_2 particles were a serious factor in increasing the hardness.[12]

The purpose of this study is to examine the microstructure, hardness and wear properties of a new Cu alloy composite namely the Cu–FeTi intermetallic composition dispersed within the matrix and grain boundaries by dissolving FeTi particles in Cu.

2. Experimental Procedure

The ferro titanium powders (72% Ti–24% Fe–4% Al; size: 48 μm) and copper powders (99.9% purity; size: 48 μm) were selected as the test materials. Cu–FeTi and zinc acetate were mixed and homogenized in an alumina laboratory ball mill for 2 h at 90 rpm and then cold pressed uniaxially with a pressure of up to 200 MPa. Zinc acetate was used to prevent cold welding and to form a precursor for the reinforcement particles. The composites and process conditions selected for the test samples are given in Table 1. Sintering temperatures were selected as 600–1000°C.

Samples were sanded using a series of SiC sandpapers from 180 grit to 2000 grit and polished with 1-μm diamond paste. For the characterization of microstructure, the samples were etched with the solution of 95% $FeCl_3$ and 5% HCl. Microstructural characterization of Cu-based FeTi-reinforced composite was made with the scanning electron microscopy (SEM; ZEISS EVO LS10) and energy-dispersive spectroscopy (EDS). Microhardness analysis was performed on a Qness Q10 M microhardness tester using a 100-g load at 0.5-mm intervals on the Vickers scale. Phase analysis with X-ray diffraction (XRD) was performed using Rigaku X-ray diffractometer, with 40-kV voltage, 40-mA current and 0.02° scanning step. The wear experiments of the samples were done on a pin-on-disc wear machine (model: UTS-Tribometer T10/20) with the loads of 10, 20 and 30 N and a sliding distance of 1200 m according to the ASTM-G65 Standard. The wear surfaces of the samples were analyzed by optical microscopy (OM; LEICA DM750).

3. Experimental Results

3.1. *Microstructural analysis*

Figure 1 describes the microstructures of composite structures. The figure shows FeTi-reinforced primary α-Cu grains together with the CuTi intermetallics. Gray areas indicated FeTi deposits and dark areas indicated α-phase. Figure 1(a) shows precipitation along the boundaries of α-phase and formation of a net-like structure after sintering at 600°C. At lower sintering temperatures, Ti deposits were homogeneously dispersed in the microstructure [Fig. 1(b)]. The structure

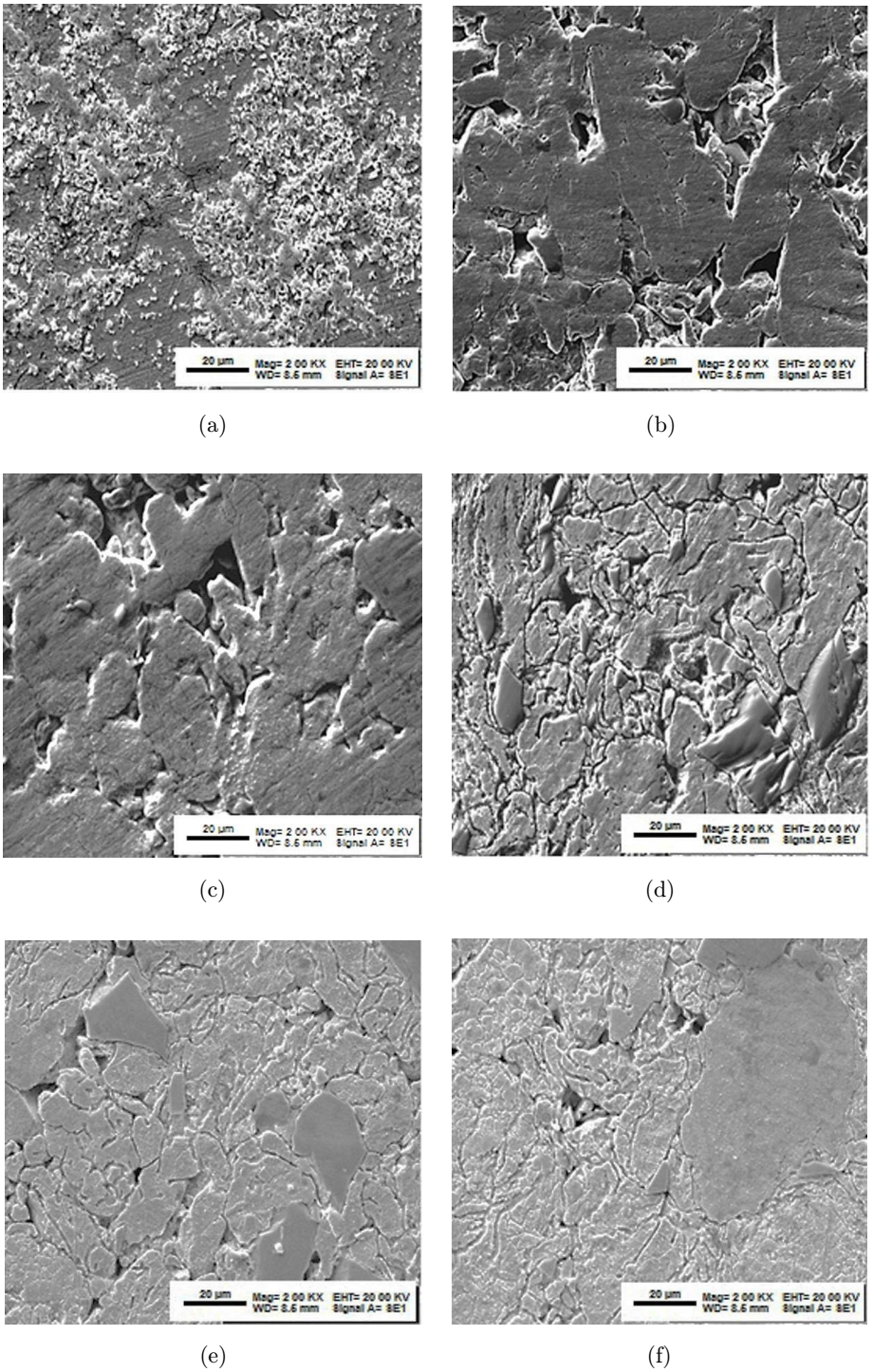

Fig. 1. SEM micrographs of the experiment samples: (a) S1, (b) S2, (c) S3, (d) S4, (e) S5 and (f) S6.

of the sample sintered at 800°C [Fig. 1(c)] was substantially different from those sintered at lower temperatures. At a sintering temperature of 800°C, the precipitates exhibited increased coarseness. The precipitates were dispersed both at the grain boundaries and within the grains. The precipitates tended to split at the primary particle boundaries at high sintering temperatures, and the grain growth

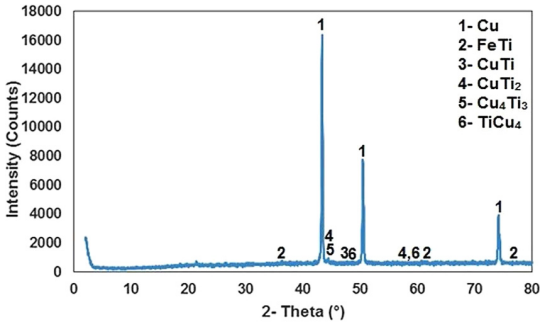

(a)

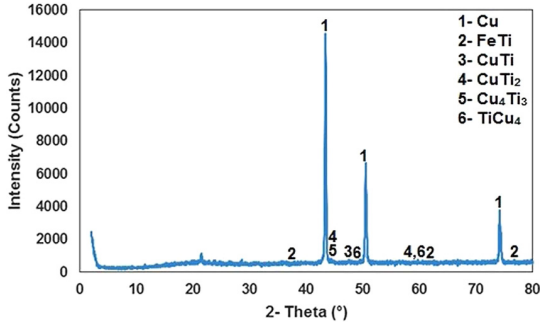

(b)

Fig. 2. XRD patterns of samples (a) S5 and (b) S12.

was limited [Fig. 1(c)]. When the sintering temperature was up to 950°C, TiCu fluid appeared and was spread at the interface. This raised the diffusion of Ti and Cu into the liquid phase.[13,14] Thus, as seen in Fig. 1(d), more liquid phase was formed and the solution of Ti–Cu intermetallics accelerated. Figures 2 and 3 confirm the presence of elements Cu (JCPDS Card No. 02-1225), Ti (JCPDS Card No. 89-5009), compounds $CuTi_2$ (JCPDS Card No. 72-0441), CuTi (JCPDS Card No. 65-2807), Cu_3Ti_2 (JCPDS Card No. 65-6822) and Cu_4Ti (JCPDS Card No. 20-0370) obtained by the XRD analyses.[15] The sintering temperature affected the interface features of diffusion between the grains and enabled the diffusion of Ti atoms. At a temperature of 950°C, the Ti–Cu intermetallic increased in size, and then decreased significantly. The dimension of the Ti–Cu intermetallic increased at a temperature of 950°C and then decreased remarkably. Due to the creation of the Ti–Cu eutectic liquid phase or the low melting point of Ti–Cu intermetallics, the Ti–Cu intermetallics were melted by the liquid composite formed during the diffusional degradation phase when the temperature was 1000°C or above. As seen in the Ti–Cu diagram,

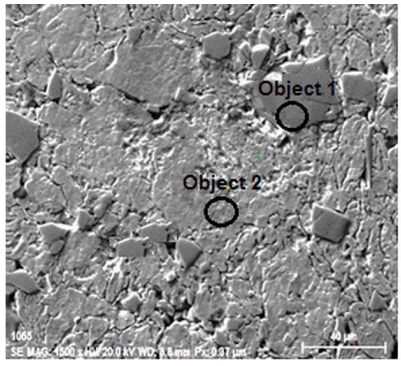

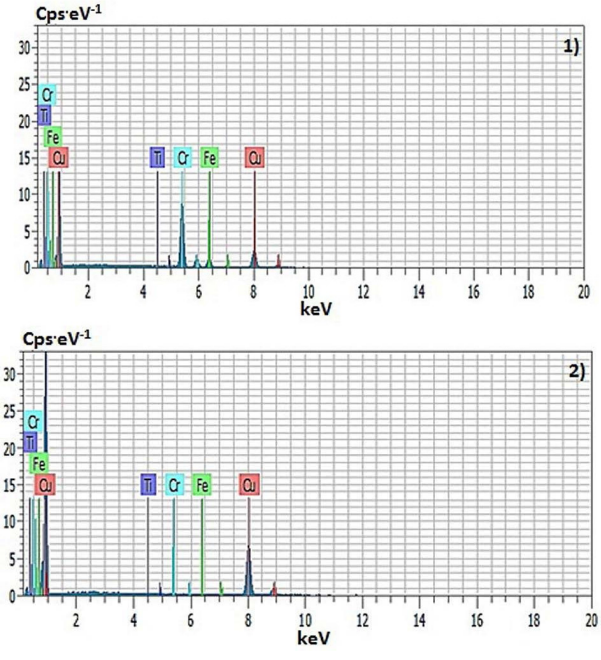

Fig. 3. EDS analysis results of the S4 sample.

a liquid phase with a low melting point above 875°C could have occurred between Ti and Cu due to the eutectic transformation. Although the eutectic point was 900°C, the eutectic structure did not have a distinctive feature. This demonstrated that no liquid phase was formed at the Ti–Cu interfaces during sintering at 950°C and below. Interface microstructure between FeTi and Cu showed a significant difference at 1000°C sintering temperature. CuTi intermetallic size was drastically reduced. As seen in Fig. 1(c), only the $CuTi_2$ phase was determined at the FeTi–Cu interface. For a sintering temperature of 1050°C, Ti–Cu compounds were absent. This showed that a liquid phase was created at 1000°C. FeTi content affected the ratio of Cu and Fe phases and the microstructure. FeTi is a hard phase and Cu is a soft

phase. With the rise of FeTi quantity, the amount of Fe phase in the composite increased and the amount of Cu decreased. It greatly changed the strength of the alloy. The number of interfaces between Fe, Ti and Cu phases increased. The grain dimensions of the two phases were significantly refined. At the same time, soft copper was evenly dispersed in the iron (Fig. 1).

The liquid phase production temperature of the Ti–Cu phase structure is not the eutectic point, but the melting temperature of the TiCu alloy.[14,16] The presence of coarse Cu_4Ti_3 particles in the matrix was inevitable. The typical structure of $CuTi_2$ phase is given in Fig. 1(b). It was determined that $CuTi_2$ with distinct grain dimensions was surrounded by CuTi and Cu_4Ti_3. The Cu_4Ti_3 phase with the same layered structure was compressed by the CuTi phases. $CuTi_2$ phases are surrounded by CuTi and Cu_4Ti_3 phases. As shown in Fig. 1, when the sintering temperature is raised to 1000°C, Cu melted locally to become liquid, but Ti remained as solid and was covered with the Cu liquid. As the temperature increased further, Ti atoms diffused into the Cu liquid, and the Ti that occurred on the surface of FeTi grains also got diffused into the Cu liquid completely. After cooling, the $CuTi_2$ crystals nucleated and expanded. When the temperature reached the highest liquid temperature of the CuTi phase (975°C), CuTi nucleated and expanded (Fig. 1). At a temperature of 950°C, the eutectic reaction $\text{Liquid} \rightarrow \text{CuTi} + \text{CuTi}_2$ occurred. $\text{Liquid} + \text{CuTi} \rightarrow \text{Cu}_4\text{Ti}_3$ peritectic reaction and growth of Cu_4Ti_3 were observed at 900°C (Fig. 1). When the solidification operation was completed, the $CuTi_2$ phase was surrounded by CuTi and Cu_4Ti_3 phases in the microstructure of the solidified Cu–Ti alloy. CuTi and Cu_4Ti_3 formed an overlapping structure. Residual stresses were detected in the grain boundaries with the precipitation of Cu intermetallic in the samples. Residual stresses might occur near the precipitate cores at the grain boundary.[16–19] Ti and Fe ratios of the samples are given in the EDS study results in Fig. 3. The Ti and Fe atoms were diffused into Cu grains by atomic diffusion. The increase in the amount of FeTi particles increased the diffusion of Ti and Fe atoms in Cu particles and increased the grain boundary intermetallics. In this case, the activation energy of Ti atoms increased and thus the diffusion ratio of Ti atoms from FeTi to the matrix increased. The spread of Ti and Fe atoms was quite high in copper above 900°C. Due to the increase in the diffusion of Ti and Fe atoms, FeTi particle size decreased in the microstructure. This resulted in an increase in the melting degree of the Cu–FeTi alloy.

3.2. *Hardness*

Microhardness curves of test samples are given in Fig. 4. Surface hardness increased due to the dissolution of FeTi particles and diffusion of Fe and Ti atoms in the structure. The hardness changed proportionally with the increase in the FeTi particles. $CuTi_2$ was fragile in nature and had the highest hardness. CuTi and Cu_4Ti_3 showed similar amounts of hardness. Cu_4Ti_3 and CuTi phases were ductile, but contained structural differences. The difference in matrix strength between Cu and Cu–FeTi was that the Cu–FeTi alloy contained a high rate of dislocation. Due to the unconformity in the thermal expansion factor and the elastic features between Cu and FeTi particles dispersed in the matrix, restricted dislocation motion occurred at the matrix–particle interface after cooling and hardness increased.[16–19] EDS analysis showed that FeTi particles are transformed into intermetallic phases due to dispersion of Cu towards the center of the particle. The diffusion of copper in titanium was faster than that of titanium in copper. Since the sizes of different atoms in the intermetallic phase did not match, most intermetallic phases had independent packed atomic structures compared to their pure elements. Thus, the diffusion of atoms in intermetallic phases was very high. Diffusion was eased by the formation of intermetallic layers.[20–22]

3.3. *Evaluation of wear behavior*

The wear performance of the Cu–FeTi alloy is displayed in Figs. 5(a) and 5(b). The composite's

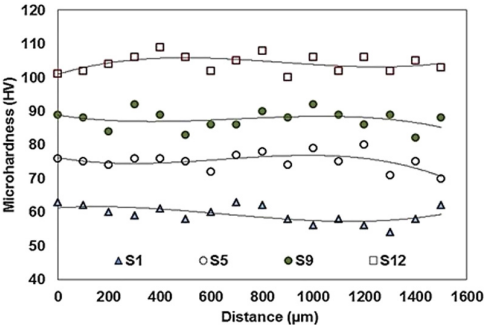

Fig. 4. Microhardness curves of test samples.

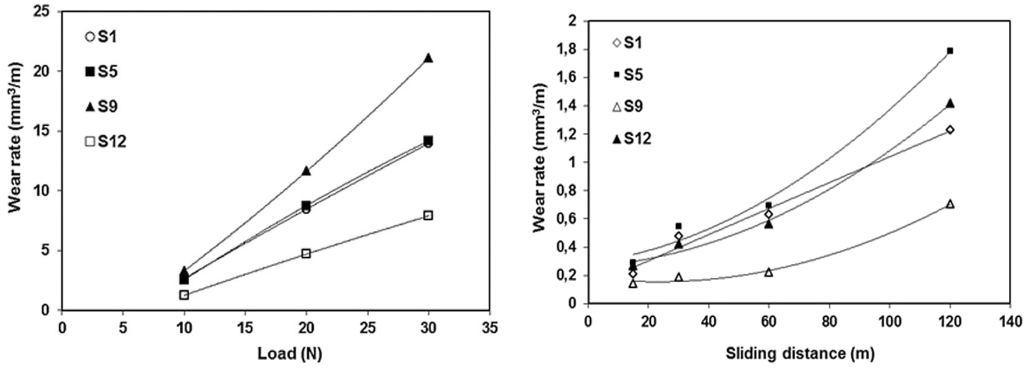

(a) (b)

Fig. 5. Wear graphs of test samples.

properties were better than those of Cu. The resulting microstructural differences, which led to the strengthening of the composite, increased the wear resistance.[23] The wear rate of the Cu–FeTi composite did not rise linearly depending on the load and distance. According to the wear data, the wear rate changes were polynomial with respect to load and sliding distance change. The intermetallic phases led to an increase in the hardness and wear resistance, but decreased ductility. Intermetallic phases with large differences in length-to-width ratio decreased the wear resistance. Intermetallic started to break during wear and increased the degree of wear.[21–24] A 76% reduction in wear of the Cu–18% FeTi was observed. As a result, the copper matrix was in direct contact with the opposing surfaces.

The wear rate of the material with each load applied was commensurate to the sliding distance from the resistive medium. This was related to the linear rule of Archard's theorem.[22] The wear quantity of the samples increased polynomially with the applied load. The increase in the amount of intermetallic phases increased the hardness and reduced the wear rate. Figures 5(a) and 5(b) demonstrate the effects of load and sliding length on the wear rate. The wear quantity of metal matrix composite (MMC) specimens increased linearly for the chosen weight ranges. From the wear quantity graphs, it was determined that the variation in sliding distance and wear rate was a polynomial function [Fig. 5(b)]. When the critical temperature was attained on the contact faces due to frictional heating, the wear changed from mild to severe.[25,26] The rate of wear increased with increasing load on all surface-treated samples. FeTi alloy had improved wear performance compared to samples without reinforcement. Wear rates of the samples were observed at 300–475 K. The plots between temperature and friction coefficient and between temperature and wear ratio for composite samples are given in Figs. 6(a) and 6(b). The friction coefficient

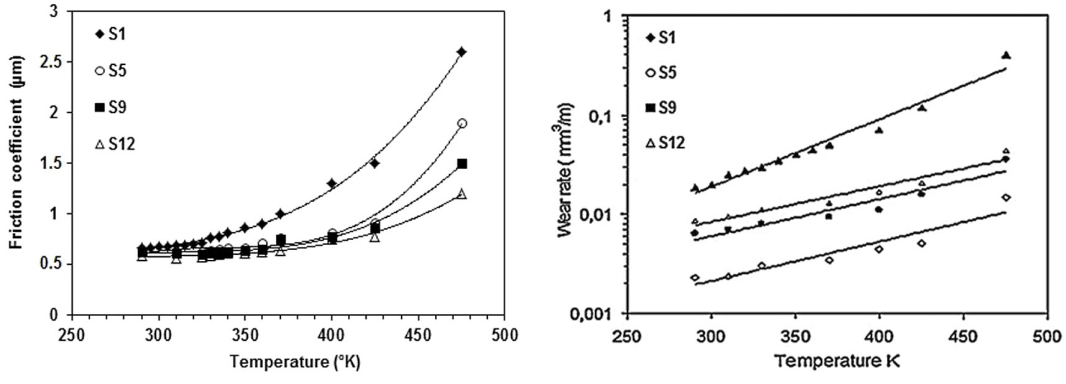

(a) (b)

Fig. 6. Plots of composite samples: (a) temperature versus friction coefficient and (b) temperature versus wear ratio.

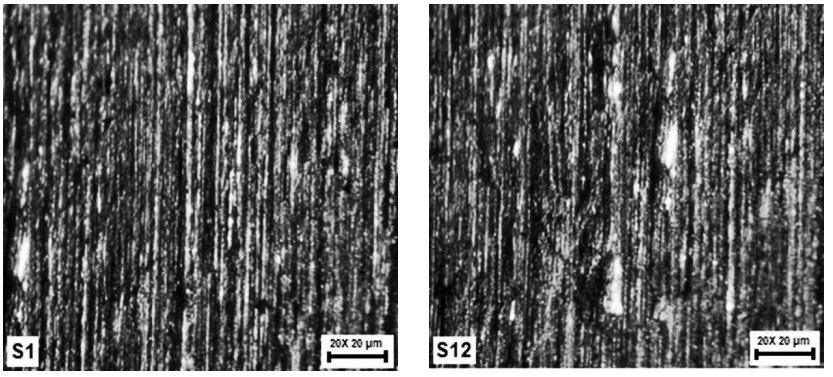

(a) (b)

Fig. 7. Wear surfaces of (a) S1 and (b) S12.

curves of the composites increased polynomially. A relationship was found between the rate of wear and the surface temperature, and between the rate of wear and the load. The features of the composites were protected up to 420 K, where a sharp transition was observed. When the temperature exceeded 375 K, the wear resistance decreased, and the friction coefficient increased rapidly. Above 420 K, the wear behaviors of the composites were very similar.

Wear surfaces of S1 and S12 are given in Fig. 7. The wear surfaces of the samples exhibited a microstructure with gutters, wear scraps and a plastering layer. The carbide particles were pulled above a specific value of temperature. Free carbides lost their ability to contribute to the load. Matrix was in touch with the opposite faces. Spills occurred as a result of the contact of the counter-abrasive surfaces with carbide and intermetallic particles. An interface separation was not detected between the particles and the matrix. There was no highly degraded material layer on the contact surface. A strong interface strength was determined.

4. Conclusions

In this study, the microstructure, hardness and wear properties of Cu-based FeTi-reinforced composites were investigated. The following results are obtained from this study:

At lower sintering temperatures, Ti precipitates exhibited a uniform distribution in the microstructure.

The structure of the alloy sintered at 800°C was significantly different from the low-temperature-sintered alloy. The precipitates had a rough appearance.

The interface microstructure between FeTi and Cu at 1000°C showed a significant difference. The thickness of the CuTi intermetallic was considerably reduced and only the $CuTi_2$ phase was detected at the FeTi–Cu interface. Ti–Cu intermetallic disappeared at 1050°C.

The increase in FeTi ratio increased the diffusion rate of Ti and Fe atoms and their ratio in Cu particles.

The hardness changed proportionally with the increase in the FeTi particles. $CuTi_2$ was fragile in nature and had the highest hardness. CuTi and Cu_4Ti_3 showed similar amounts of hardness.

The morphology of intermetallic phases led to higher hardness and wear strength.

FeTi reinforcement was effective in increasing the wear resistance of Cu-based FeTi alloy.

A 75% reduction in wear rate was achieved by adding 18-wt.% FeTi to pure copper.

Acknowledgments

The authors are grateful to Kayalar Copper Alloys Industry and Trade, Inc. for their assistance in conducting the experiments.

References

1. A. H. Cai, D. W. Ding, W. K. An, G. J. Zhou, Y. Luo, J. H. Li and Y. Y. Peng, *Mater. Chem. Phys.* **151** (2015) 243.
2. S. W. Lee, S. C. Lee, Y. C. Kim, E. Fleury and J. C. Lee, *J. Mater. Res.* **22** (2007) 486.
3. S. Pauly, J. Das, J. Bednarcik, N. Mattern, K. B. Kim, D. H. Kim and J. Eckert, *Scr. Mater.* **60** (2009) 431.

4. A. H. Cai, D. W. Ding, X. Xiong, Y. Liu, W. K. An, G. J. Zhou, Y. Luo, T. L. Li, H. Wang and Y. Wu, *Mater. Sci. Eng. A* **588** (2013) 49.
5. S. Pauly, J. Das, C. Duhamel and J. Eckert, *Metall. Mater. Trans. A* **39** (2008) 1868.
6. A. Elrefaey and W. Tillmann, *J. Mater. Process. Technol.* **209** (2009) 2746.
7. S. Kundu, M. Ghosh, A. Laik, K. Bhanumurthy, G. B. Kale and S. Chatterjee, *Mater. Sci. Eng. A* **407** (2005) 154.
8. M. Konieczny, *Mater. Lett.* **262** (2008) 2600.
9. C. Li, J. Xia and H. Dong, *Wear* **261** (2006) 693.
10. K. W. Ng, H. C. Man and T. M. Yue, *Appl. Surf. Sci.* **254** (2008) 6725.
11. M. Guo, K. Shen and M. Wang, *Acta Mater.* **57** (2009) 4568.
12. D. Božić, J. Stašsić, J. Ružić, M. Vilotijević and V. Rajković, *Mater. Sci. Eng. A* **528** (2011) 8139.
13. C. Colinet, A. Pasture and K. H. J. Buschow, *J. Alloys Compd.* **247** (1997) 15.
14. J. L. Murray, *Binary Alloy Phase Diagrams*, 2nd edn., Vol. 2 (ASM International, Metals Park, 1990).
15. H. Okamoto, *J. Phase Equilib.* **23** (2002) 549.
16. F. Zhou and Z. Li, *Acta Metall. Sin.* **36** (2000) 171.
17. S. Nagarjuna, M. Srinivas, K. Balasubramanian and D. S. Sarma, *Acta Mater.* **44** (1996) 2285.
18. S. Semboshi, T. Nishida and H. Numakura, *Mater. Sci. Eng. A* **517** (2009) 105.
19. A. E. W. Jarfors, *J. Mater. Sci.* **34** (1999) 4533.
20. M. B. N. Shaikh, S. Arifa, T. Aziz, A. Waseem, M. A. N. Shaikh and M. Ali, *Surf. Interfaces* **15** (2019) 166.
21. Y. D. Zhu, M. F. Yan, Y. X. Zhang and C. S. Zhang, *Comput. Mater. Sci.* **123** (2016) 70.
22. S. Suzuki, K. Hirabayashi, H. Shibata, K. Mimura, M. Isshiki and Y. Waseda, *Scr. Mater.* **48** (2003) 431.
23. M. R. Bateni, F. Ashrafizadeh, J. A. Szpunar and R. Drew, *Wear* **253** (2002) 626.
24. M. B. N. Shaikh, T. Aziz, S. Arif, A. H. Ansari, P. G. Karagiannidis and M. Uddin, *Surf. Interfaces* **20** (2020) 100598.
25. L. Shen, Z. Li, Q. Dong, Z. Xiao, M. Wang, P. He and Q. Lei, *Tribol. Int.* **92** (2015) 544.
26. C. Guo, J. Zhou, Y. Yu, L. Wang, H. Zhou and J. Chen, *Mater. Des.* **36** (2012) 482.
27. C. L. Chu and S. K. Wu, *Scr. Metall. Mater.* **33** (1995) 139.